Phobos Image Enhancement using Unpaired Multi-Frame Acquisitions from Indian Mars Color Camera

Indranil Misra*, Litu Rout, Sunita Arya, Yatharath Bhateja, S Manthira Moorthi and Debajyoti Dhar

Signal and Image Processing Group,

Space Applications Centre, Indian Space Research Organisation,

Ahmedabad, Gujarat, India

Corresponding Author E-Mail Address: misra.indranil@gmail.com

Abstract

The Mars Color Camera (MCC) of Indian Space Research Organisation (ISRO) captures the elusive moon of Mars, Phobos. MCC instrument is the eye of Mars Orbiter Mission (MOM) launched by ISRO on 05th November 2013 from the spaceport of India, Sriharikota. MCC has already provided more than 1000 images of Martian surface features covering different terrains. Recently, MCC has captured Phobos image at successive time instances on 01st July 2020. Multiple unpaired acquisitions of planetary remote sensing images often contain rich information to super resolve the spatial details of these images. This paper describes the techniques developed to enhance the Phobos image from MCC multi-frame acquisitions using image rectification and topographic data. In this regard, the co-registration of MCC frames is a crucial step. To co-register the data at sub-pixel level, we present a method, namely Random Sample Consensus (RANSAC) pruning based Scale Invariant Feature Transform (R-SIFT). The image composite is based on Medoid approach. It is further enhanced by contrast limited adaptive histogram equalization

(CLAHE). The location of Phobos is computed using Spacecraft Planet Instrument Camera Matrix Event (SPICE) toolkit. For topographic correction, we rely on the Digital Elevation Model (DEM) of Phobos using publicly available resources. Visual inspection and image quality parameters, such as BRISQUE, RMSE, PSNR, and SSIM are estimated for both enhanced and topographically corrected image for assimilation purpose. After incorporating these techniques, the final Phobos image appears more representative, spatially enhanced, and has normalized radiometry to study its surface features.

Keywords: Image Registration, Medoid, SPICE, Topographic Correction, Enhancement, Mars Color Camera.

1. Introduction

Phobos is the natural satellite of Mars that orbits at around 6000 kilometers from Martian surface. Different spacecraft missions towards Mars have captured several unique perspectives of Phobos. It has been observed by Mars Flyby missions, such as Mariner 9 spacecraft [1] launched in 1971. The multi-temporal acquisitions by different Mars Missions are intended to enrich our knowledge of Phobos. Among these, Mars Reconnaissance Orbiter (MRO) [2] spacecraft captures over 100 images of Phobos using High Resolution Imaging Science Experiment (HiRISE) and the hyper-spectral infrared Compact Reconnaissance Imaging Spectrometer for Mars (CRISM). High Resolution Stereo Camera (HRSC) [3] onboard European Mars Express Mission [4] is capable of imaging planetary bodies at a resolution of 40 meters per pixel from a distance of 1000 km. The Mars Express mission allows the spacecraft to perform close flybys to capture largest Martian moon Phobos [5]. As per the simulation models, Phobos is composed of a mixture of materials from Mars and impactor [6]. The science experiments are carried out using different types of data

to find the nature of Phobos interior [7]. Recent studies indicate that Phobos can be accreted from an impact generated disk, and it is found that that the building blocks of Phobos mostly come from Martian mantle [8]. Mapped by multiple remote sensing images, it is also established that Phobos has an irregular shape [9].

Indian Mars Color Camera (MCC) onboard Mars Orbiter Mission (MOM) has got an opportunity to image Phobos in July 2020 [10]. MCC is a RGB Bayer pattern camera that operates in visible range (0.4 µm to 0.7 µm). MCC detector array has 2048x2048 elements on a pixel pitch of 5.5µm [11]. MCC has attempted nine successive imaging shots to capture Phobos on 01st July 2020. Out of nine, six frames captured Phobos that is completely within the field-of-view (FOV) of MCC. During the imaging session, the distance between MOM and Phobos varies between 4200 km to 4330 km. The estimated spatial resolution of these frames ranges from 210 meters to 217 meters. While earlier acquisitions on 14th Oct 2014 during Mars surface imaging had relatively small Phobos images, the recent acquisition has gathered more spatial information that offers essential surface details of this mysterious moon. The latest MCC Phobos images helps planetary researchers to improve the study on surface geological characteristics and infer the changes happened in crater morphology. Figure-1 shows the MCC imaging of Phobos at six different time stamps in an ascending imaging orbit. The imaging time shown in Figure-1 is in Coordinated Universal Time (UTC).

MCC Bayer pattern images are received on ground at ISRO Space Science Data Center (ISSDC) at Byalalu, India and processed to reconstruct full color RGB images using the demosaicking process [12,13]. MCC images are packed with all relevant imaging meta

information in Planetary Data Standard (PDS) for further processing by the end user [14]. Multiple frames of MCC containing Phobos creates a dire need to generate an enhanced Phobos image using image processing techniques. This paper highlights the image registration process developed for multiple frames of MCC. Further, it estimates the registration accuracy both qualitatively and quantitatively [15]. The composite generation and image enhancement technique is described in section-4 to generate a more representative Phobos image [16]. SPICE computation flowchart using different kernels to compute location, distance and resolution is elaborated in the subsequent sections [17]. Finally, topographic correction [18] step is performed to normalize the radiance of the composite image. The image quality is quantified using both no reference metrics and Phobos map reference of United States Geological Survey (USGS) for better understanding. The surface features of Phobos are easily identified in MCC enhanced image with the help of Phobos nomenclature map [19]. The final goal of implementing this data processing pipeline is to improve the spatial information of a planetary image using unpaired data, which can be re-used to create new digital image model of Mars using latest acquisitions.

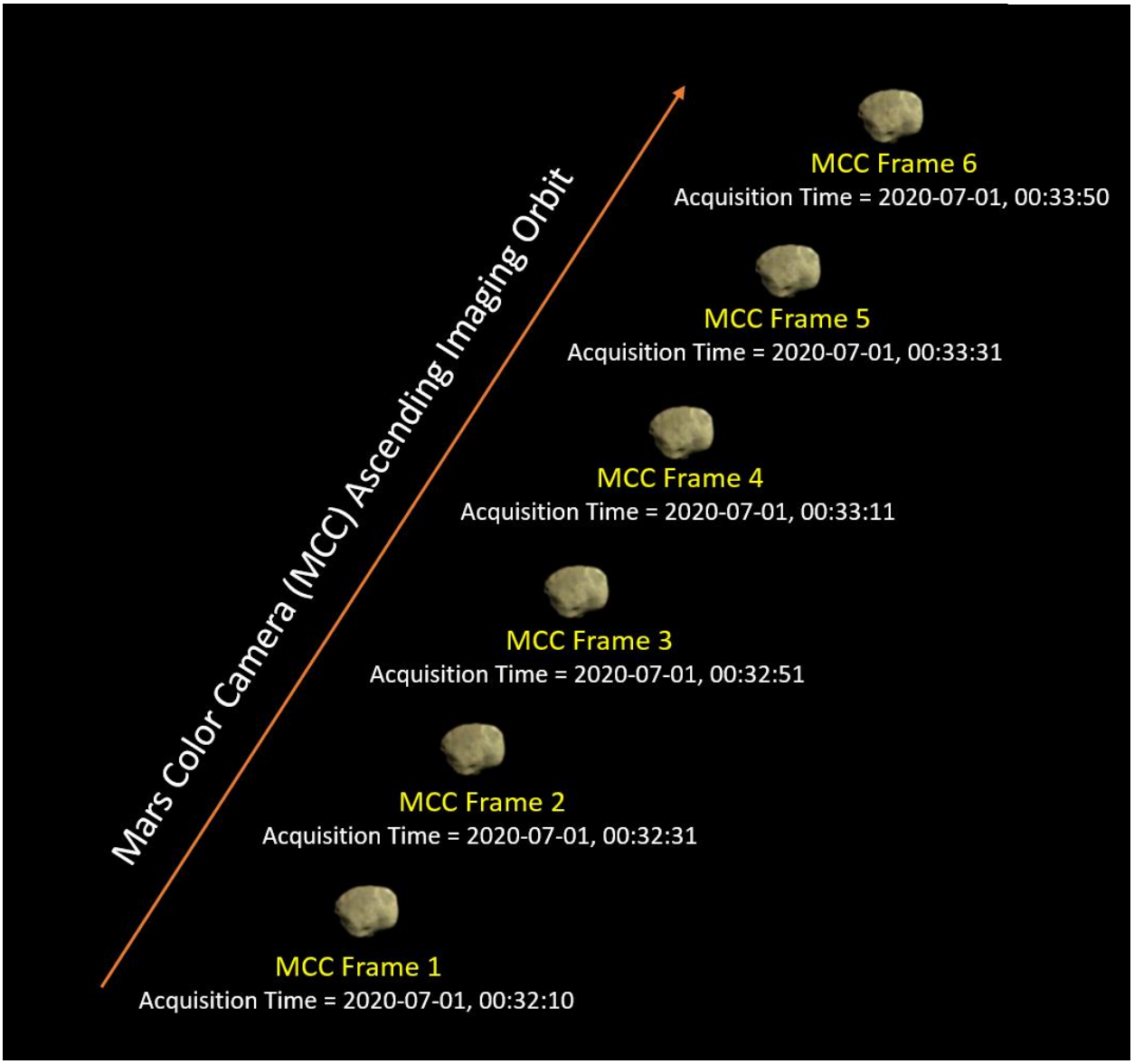

Figure-1: Multiple instances of Phobos in ascending orbit as captured by MCC.

2. Review of Related Work

Remote Sensing image enhancement using unpaired images requires multiple image processing techniques at different stages in a coordinated manner. In this regard, planetary data processing software, such as Integrated Software for Imager and Spectrometer (ISIS) [20] and Ames Stereo processing pipeline [21] provide software routines to align and enhance the planetary remote

sensing images. But multi-temporal image co-registration is a challenging task for planetary images due to lack of textual information, low contrast and uneven illumination characteristics [22]. Feature based image matching provides a way to establish the correspondence between two images. Different detection techniques, such as Harris [23], SURF [24], ORB [25], and SIFT [26] are used to solve the matching problem. While SIFT is computationally intensive, it is a powerful feature detector that is invariant to illumination, rotation and scaling. Furthermore, SIFT can generate stable spatial relationship in planetary images because it can describe a key point with a local feature vector [26, 27]. For this reason, it is often employed to achieve high precision co-registration in planetary images [28]. However, it has been observed to have spurious matched points, which are detected in optical remote sensing images using SIFT. It is important to eliminate these spurious points for effective estimation of useful parameters in co-registration [29]. Therefore, the amalgamation of a correct matching technique with proper optimization model is essential for planetary image co-registration. Essentially, it opens a series of new challenges to solve the image co-registration problem.

The generated composite image using multi-temporal acquisitions is usually a better representation than its individual counterparts. In spatial data mining and clustering, medoid based approach is found to be quite effective for information discovery [30, 31]. In remote sensing domain, medoid approach is explored for classifying Landsat images and for generation of annual thematic maps [32]. To the best of our knowledge, medoid for composition is relatively less explored to generate a representative image in planetary science, which we wish to explore in this study. It is worth mentioning that planetary images require further improvements to study the surface features and morphology. To this end, some researchers use correlated noise to enhance

planetary images, which may identify previously unresolved Aeolian terrain of Mars [33]. However, this technique requires pure spectrum data from multiple wavelength channels, and it is not suitable for Bayer pattern camera like MCC. Furthermore, relatively less attention is paid towards planetary image enhancement to retrieve more topographical details and improve the image interpretation. In this paper, we intend to provide a comprehensive approach for the enhancement of planetary images.

3. MCC Frames Co-Registration

MCC has captured the image of Phobos in six frames. Each frame has different time of acquisition and viewing geometry. Table-1 shows PDS file name and image frame acquisition time of MCC Frames. The PDS file name points to the detached label containing description of the data products used in our experiments. The PDS file naming convention starts with instrument name "MCC", followed by mission phase, data type, and imaging mode. The long number string denotes the observation time of the MCC frame. The last five characters recognize the PDS data type and station id where data was acquired [34]. To generate a composite using these frames, the first task is to co-register the MCC frames while keeping one frame as a reference. Since Frame 3 is in the middle of the acquisitions, it is chosen as the reference for co-registration. The technique developed for feature matching and optimization is built upon Random Sample Consensus (RANSAC) pruning based Scale Invariant Feature Transform (R-SIFT) [26, 35].

Table-1: MCC Frames Data Details used for our study

MCC Frames	PDS File Name	Frame Acquisition Time
Frame 1	MCC_MRC_20200701T003210065_D_D32	2020-07-01, 00:32:10
Frame 2	MCC_MRC_20200701T003231066_D_D32	2020-07-01, 00:32:31
Frame 3	MCC_MRC_20200701T003251066_D_D32	2020-07-01, 00:32:51
Frame 4	MCC_MRC_20200701T003311067_D_D32	2020-07-01, 00:33:11
Frame 5	MCC_MRC_20200701T003331068_D_D32	2020-07-01, 00:33:31
Frame 6	MCC_MRC_20200701T003350068_D_D32	2020-07-01, 00:33:50

3.1 R-SIFT based Matching Technique

SIFT is one of the popular detection and description techniques for automatic remote sensing image registration [36]. It detects relevant features and provides a description using a vector of 128 elements. It creates scale space extrema using Gaussian Kernel. Difference of Gaussian (DOG) pyramid is created to locate minimum and maximum around a neighboring point across the scales. It extracts stable key points at sub-pixel level localization. The Gaussian relation between Smooth Image (L) and Input Image (I) at point (x, y) is established using the following equation:

$$L(x, y, \sigma) = G(x, y, \sigma) * I(x, y) \qquad (1)$$

$$where\ G(x, y, \sigma) = \frac{1}{2\pi\sigma^2}\left(e^{-\frac{x^2+y^2}{2\sigma^2}}\right) \qquad (2)$$

On many occasions, matched feature points contain outliers which need to be eliminated for better estimation of transformation parameters [37, 38]. RANSAC approach is used to prune the set of control points. It usually operates in two steps: hypothesis generation from random samples and hypothesis evaluation by verifying the samples whose error from the chosen hypothesis is within a predefined threshold [39]. This procedure is repeated for a fixed number of iterations,

each time producing either a model, which is rejected because too few points are classified as inliers, or a refined model together with a corresponding error measure. Once the inlier candidates reach the threshold level the refined transformation model is generated and saved for further processing. With failure probability α, the number of iterations that is enough to pick all inlier samples at least once is given by:

$$N = \frac{\log \alpha}{\log(1-\gamma^m)}, \qquad (3)$$

where m is the number of data points to generate a hypothesis, γ is the probability of picking up an inlier, i.e., ratio of inliers to whole sample data (inliers ratio).

Inlier ratio plays a critical role in selection of stable set of match points and reject the outliers to estimate the transformation model. In our case, inlier ratio is chosen as 0.8, which gives optimum performance for the MCC frames. The affine transform parameters are estimated with pruned matched points and used to resample the individual frames in order to generate co-registered frames. The technique developed for co-registration is presented as an automatic processing workflow in Figure-2. The data preprocessing stages identify the Phobos imaging region in all the frames and extract the overlap region. The frames are then transformed to bring it to the common image plane for image rectification, such that all the frames have same size. Auto-registration stage assumes Frame 3 as reference and all other frames as input to co-register with the reference frame. SIFT matching and RANSAC outlier rejection generate matched control points, which is used to estimate the transformation parameters. The input frames are resampled to generate co-registered frame stack. The intermediate steps for data preparation and co-registration of MCC frames is described below:

Algorithm 1

1. *Region of Interest (ROI) Identification from MCC Frames.*
2. *Geometric transformation of MCC frames to bring the images in common plane with fixed size.*
3. *Common Overlap area extraction from all frames.*
4. *SIFT based Feature Detection and Description.*
5. *Random selection of the minimum number of SIFT matched points required to determine the model parameters.*
6. *Solve for the parameters of the transformation model.*
7. *Determine how many points from the set of all points fit with a predefined tolerance.*
8. *If the fraction of the number of inliers over the total number of points in the set exceeds a predefined threshold, estimate the model parameters using all the identified inliers.*
9. *Otherwise, repeat steps 5 through 8 for maximum N times.*
10. *Resample the MCC frames to co-register the data.*

3.2 Visual Inspection of Co-Registration Performance

The co-registration framework is used to register the MCC frames that contains Phobos. The image in each frame is shifted with respect to the reference frame in different magnitude across both directions. Figure-3 shows the mis-alignment in MCC RGB frames and Red band of MCC Frame 3 (one band of reference frame is shown for visualization) before correction. Co-Registered MCC frames are aligned at sub-pixel level and can be easily viewed in Figure-3 by horizontal swipe between input and reference frame.

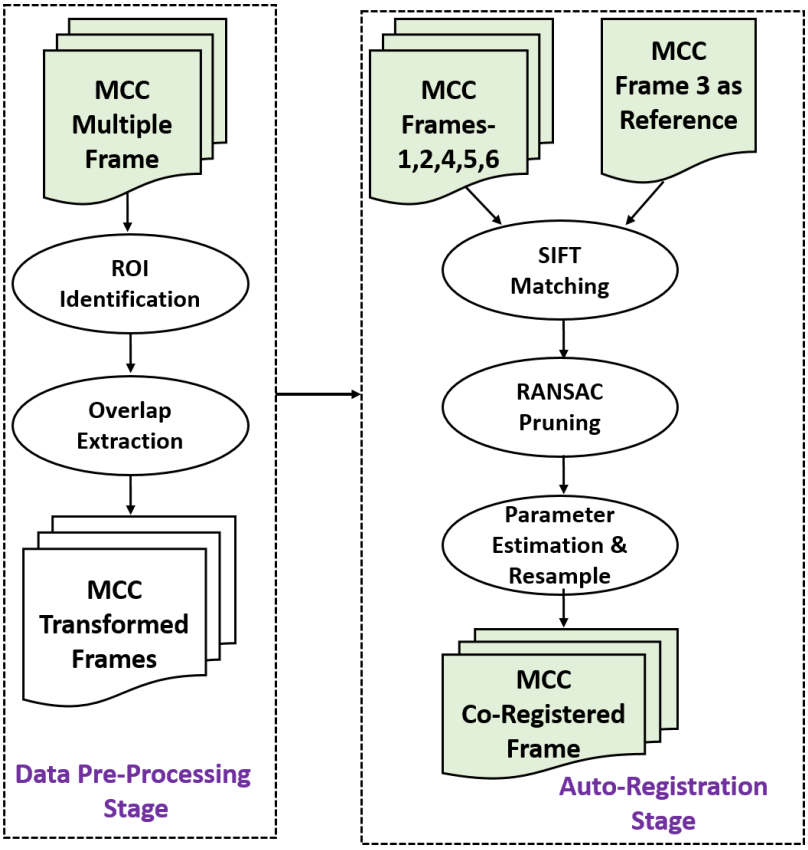

Figure-2: MCC co-registration processing workflow.

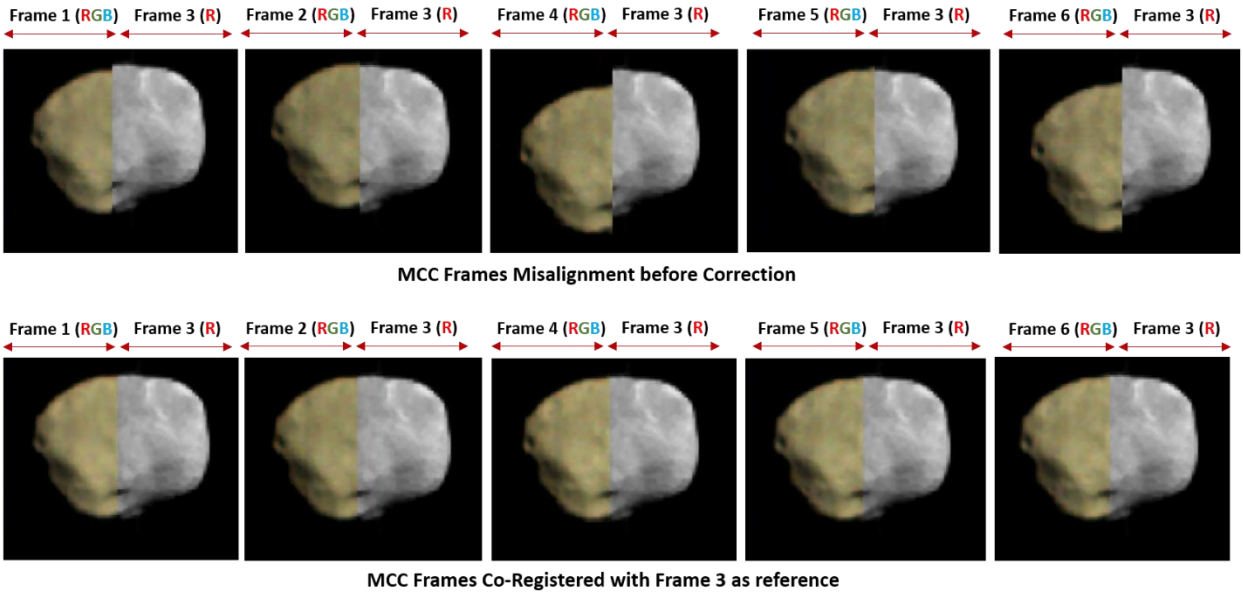

Figure-3: Co-Registration of MCC frames using R-SIFT based feature matching technique

3.3 Quantitative Evaluation of Co-Registered MCC Frames

The pixel shift of input MCC frames with respect to reference Frame 3 is computed in both horizontal and vertical direction by R-SIFT based matching as described in section 3.1. The number of matched points are well distributed over the image to compute average shifts in both the directions before and after correction (shown in Table-1). It has been found that sub-pixel level co-registration accuracy is achieved in the output co-registered MCC Frames.

To evaluate the performance of automatic co-registration technique using another metric, registered MCC frames are again correlated with R-SIFT using same reference. The root mean square error (RMSE) is calculated using pruned control matched points that are obtained from the developed framework. RMSE is often considered as an appropriate metric to represent the performance of a co-registration model [40]. Table-2 shows final RMSE error computed for each output MCC frames with respect to the reference frame. RMSE is computed as follows:

$$RMSE = \sqrt{\left(\frac{1}{N}\sum_{i=1}^{N}\left\|X_i - \hat{X}_i\right\|^2\right)}, \qquad (4)$$

where N represents the total number of matched points,

X_i is the (x_i, y_i) coordinates in the MCC Frame 3 (Reference),

$\hat{X}_i$ is the $(\hat{x}_i, \hat{y}_i)$ estimated coordinates based on the final transformation model of output MCC frame. Observe the reductions in pixel shift after co-registration.

Table-2: Evaluation of MCC co-registration by computing pixel shifts and final RMSE.

MCC Frame Number	**Input Shift in Horizontal Direction (in pixel)**	**Input Shift in Vertical Direction (in pixel)**	**Output Shift in Horizontal Direction (in pixel)**	**Output Shift in Vertical Direction (in pixel)**	**Number of pruned matched points**	**RMSE Error (in pixel)**
Frame:1	3.07	2.69	-0.24	0.10	22	0.18
Frame:2	1.54	-1.72	-0.22	-0.05	36	0.15
Frame:3	***Reference Frame***					
Frame:4	0.87	10.01	-0.15	-0.21	28	0.20
Frame:5	5.03	-1.64	-0.11	-0.23	25	0.17
Frame:6	2.47	9.09	-0.08	-0.36	31	0.28

4. Composite Generation and Enhancement

MCC Co-Registered frames are composed together to generate a Phobos image that is more representative than the individual frames. To generate a representative composite, the "medoid" is computed, which is the middle of the radiometric measurement of a particular pixel among multiple pixel values from MCC frames [41]. It is a measure of the center of multi variate set of points similar to median in univariate set [42,43]. This approach generates most radiometrically consistent composite images. From mathematical perspective, medoid is defined as follows for the generation of MCC composites:

$$Medoid\ (k) = arg\ \min_{x_j}\ \left(\sum_{i=1}^{n} \left\| x_j - x_i \right\|\ \right), \qquad (5)$$

where k = MCC pixel location,

x_j = pixel value under consideration for medoid,

x_i = pixel value in that location at other MCC frame,

n = No of pixel values at a particular location (Here, n is fixed to 6 as per the number of MCC frames),

min= minimum operator selects the pixel value from the MCC frames that minimizes the expression.

The medoid composite of Phobos image is a rich representation of multiple MCC frames. It is enhanced further with contrast limited adaptive histogram equalization (CLAHE) to enhance the local features in the composite image [44]. The CLAHE based image enhancement limits the amplification of the contrast stretch based on the pre-defined histogram limit [45,46]. Here, one of the important parameters is the window size around a pixel for which histogram is equalized. The windows size is set to 128 for CLAHE enhancement of MCC composite, which is experimentally found to give an optimal visual appearance. Figure-4 shows the MCC individual frame, Medoid composite and CLAHE based enhancement on MCC composite. MCC Frame 3 is chosen as the reference individual frame. MCC medoid composite captures the representative features of Phobos terrain, and the enhancement by CLAHE improves the contrast of local features at different locations.

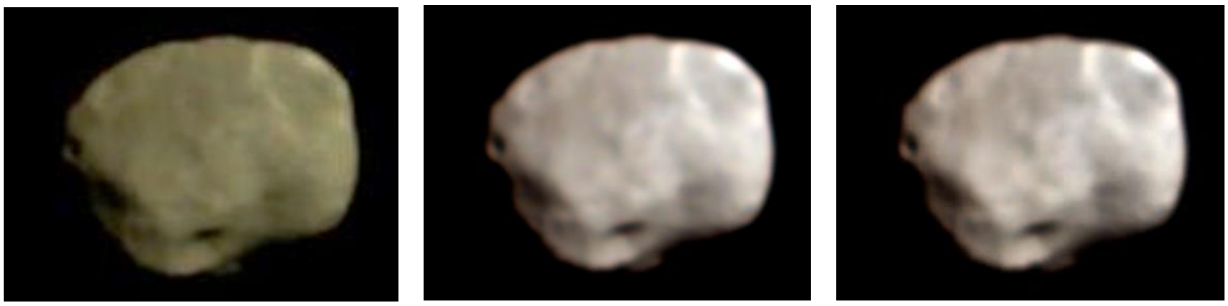

Figure-4: MCC Phobos image as Medoid composite that is enhanced further by CLAHE.

Table-3: MCC composite image quality performance.

S.No	MCC Image	BRISQUE Model Score
1.	MCC Individual Frame	60.98
2.	MCC Medoid Composite	56.95
3.	MCC Enhanced CLAHE Composite	53.75

As there is no reference image to compare, blind/reference-less image spatial quality evaluator (BRISQUE) score is computed for all the three images shown in Figure-4. BRISQUE uses scene statistics to quantify the distortion and provides a holistic measure of image quality [47]. Table-3 shows BRISQUE score that indicates MCC Enhanced CLAHE composite has better image quality than medoid composite and individual frame.

5. SPICE Computation for Geometrical Parameter Retrieval

The central location and distance from which MCC captured Phobos is pivotal to identify the features in the image. In addition, it is essential to determine the spatial resolution of the data. The geometrical parameters of Phobos images is derived using SPICE toolkit. SPICE provides a medium to determine observation geometry and enhance the information about the image for further processing [48]. The SPICE kernels are structured parameter files that describe the ephemeris and attitude of the spacecraft, the spatial orientation of the instrument and physical parameters of the celestial bodies in the solar system. It provides the relationship between spacecraft time and time as measured on the planet. Furthermore, it offers the provision to determine the location of the target body. These kernel files are used with the SPICE software library. It contains functions that perform geometric computations for space science missions and astronomical applications to recover full value of the acquired data [49].

The SPICE library is now used worldwide for different planetary missions including MOM [50]. We have used SPICE C Implementation known as “CSPICE” Version No: N0066 in the reported experiments. The main goal of SPICE computation in our task is to determine the center latitude and longitude of the captured Phobos image. In addition, it is intended to estimate the distance from MCC at the time of imaging. The solar and photometric angles, such as incidence angle, emission angle, and phase angle assist in determining the vital imaging conditions and correct the planetary remote sensing data accordingly. To compute the required geometrical parameters at a given instant of time, all the necessary kernel files are given to the SPICE toolkit. Figure-5 describes the set of inputs to compute the required geometrical parameters using SPICE toolkit.

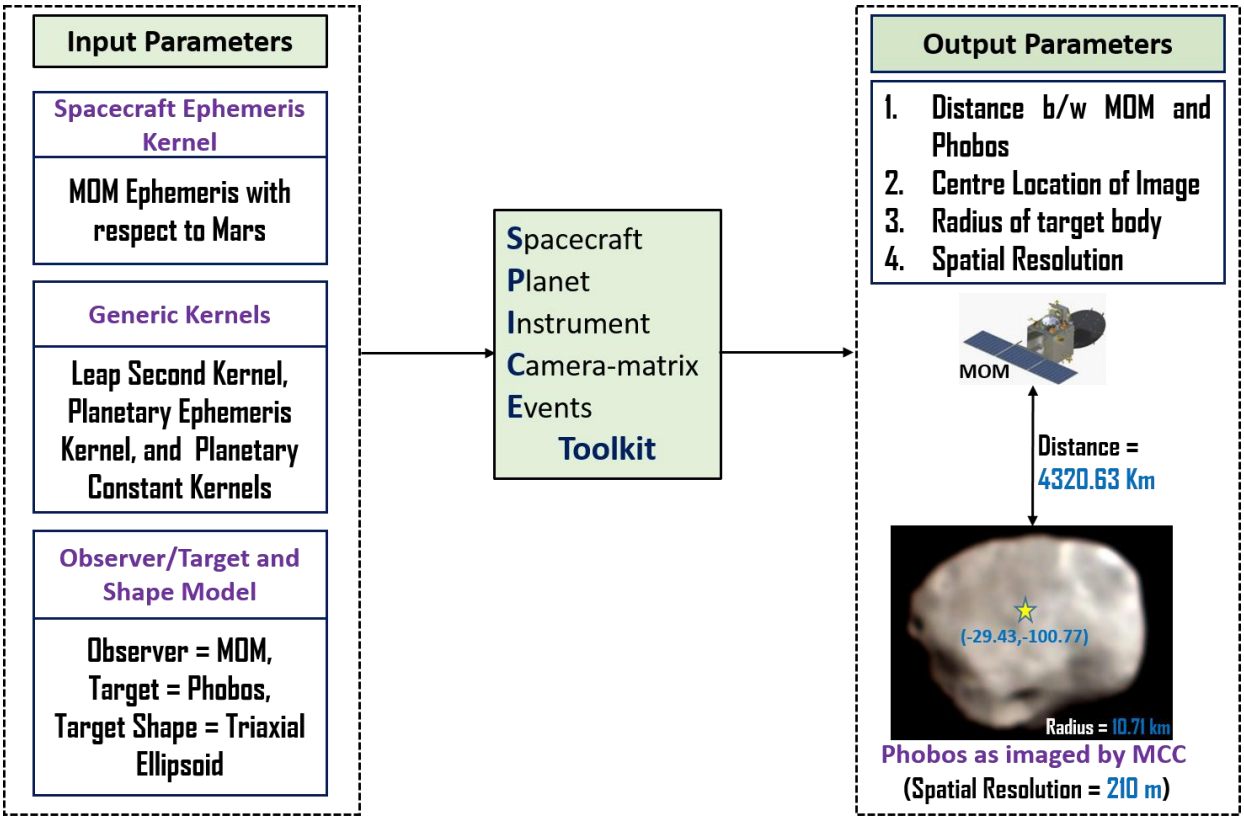

Figure-5: Flowchart for MCC Geometrical Computation of Phobos image using SPICE toolkit

We have taken MCC frame 3 (reference frame) imaging time, which is the middle frame of the acquisitions for computation of geometrical parameters. At MCC Phobos imaging time 01 July 2020 00:32:51:0000 UTC, estimated distance between MOM and Phobos is found to be 4320.63 Kilometers. In our computation, we have assumed target shape of Phobos to be triaxial ellipsoid and computed radius found to be 10.71 Kilometers. Further, the center latitude and longitude are estimated to be -29.43 Degree and -100.77 Degree, respectively. Using MCC detector size and computed distance between MCC and Phobos, the spatial resolution of captured Phobos image is found to be around 210 meters.

6. Topographic Correction of MCC Phobos Image

Phobos region captured by MCC contains lot of undulation in terrain, which results in topography shading and affects the radiometry of the image. Radiometric spectral signature is hampered by topographic effects especially on the rugged terrain of Phobos [51]. The effect of topography can be corrected using Digital Elevation Model (DEM) and solar illumination angles so as to normalize the radiometry of planetary remote sensing images. DEM is required to compute terrain slope and aspect angle [52]. Surface Normal is derived using slope and aspect that flows as an input to compute solar illumination angles at every pixel. Solar Azimuth and Solar elevation is computed using SPICE, which is also needed to compute the illumination angle. The local solar illumination angle β is defined as follows:

$$\cos\beta = \cos\lambda\cos\Phi + \sin\lambda\sin\Phi\cos(\Theta_a - \Theta_b), \qquad (6)$$

where λ = terrain slope, Φ = solar zenith angle, Θ_a = solar azimuth, Θ_b = topographic azimuth (aspect angle).

Once illumination angle is computed for the whole image at every pixel element, a normalized radiance value can be computed using Lambertian cosine terrain correction. The cosine correction algorithm is chosen to correct the topography effects in the enhanced composite image of Phobos as it doesn't require much external parameters for computation [53].

$$\rho_H = \rho_T \left(\frac{\cos\Phi}{\cos\beta}\right), \qquad (7)$$

where ρ_H = radiance of horizontal surface, ρ_T = radiance of inclined (terrain), β = solar illumination angle, Φ = solar zenith angle.

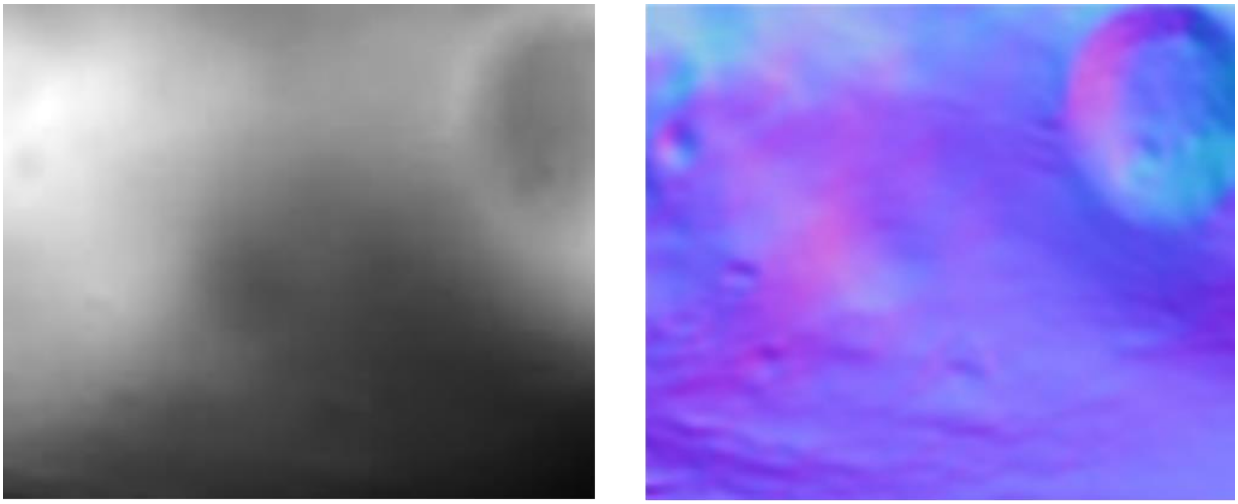

Phobos DEM Surface Normal

Figure-6: Extracted DEM and computed surface normal of Phobos for topographic correction

Phobos DEM is readily available by USGS at 100 meters per pixel resolution [54]. The DEM is generated using European Space Agency High Resolution Stereo Camera (HRSC) onboard Mars Express spacecraft. The DEM is extracted as per MCC imaging area, and the corresponding surface normal is used for topographic correction. Figure-6 shows extracted Phobos DEM and corresponding surface normal.

For clarity, the processing framework for topographic correction of Phobos image is shown in Figure-7. The pipeline is divided into two stages. The data preparation stage orients MCC enhanced image to Phobos DEM map such that the common area is extracted between MCC and Phobos Global DEM. MCC-DEM registration is based on R-SIFT matching technique as described in section-3 to generate MCC Composite aligned image. The topographic correction stage initiates with slope and aspect angle computation from the extracted DEM of Phobos. SPICE is used to retrieve the solar angles using MCC image meta details. Finally, the cosine based terrain correction takes aligned image, surface normal, and solar angles to generate topographically corrected image.

The algorithm steps of topographic correction framework is as follows:

Algorithm 2

1. *Phobos DEM is resampled to MCC image resolution, i.e., 210 meters.*
2. *MCC image is rotated clockwise 12 degrees to make it map oriented.*
3. *Overlap area is extracted between MCC image and Phobos DEM.*
4. *MCC image is aligned over DEM using R-SIFT based feature matching.*
5. *Terrain slope and aspect angle are computed from extracted DEM.*
6. *Surface normal is estimated using slope and aspect.*
7. *Solar angle is computed using SPICE toolkit.*
8. *Compute solar illumination angle at every pixel using equation-6.*
9. *Cosine terrain is corrected using equation-7 to generate normalized radiance of Phobos image.*

Figure-8 shows enhanced composite image of Phobos and results after topographic correction. The topographic correction creates better demarking of different target features. Limtoc crater, which is inside the circumference of Stickney is clearly visible in the topographically corrected image. Overall, it contains more details about the surface features of Phobos and reduces the topographic effects especially in highly undulating terrains. Further, it applies corrections uniformly and demarks the albedo features, such as flow channels and crater boundaries. The magnified image shows that Limtoc (green bounding box) and Wendell (yellow bounding box) features are well resolved in the corrected images. The comparison between MCC composite image and topographically corrected image also shows that the spectral characteristics are also preserved after correction.

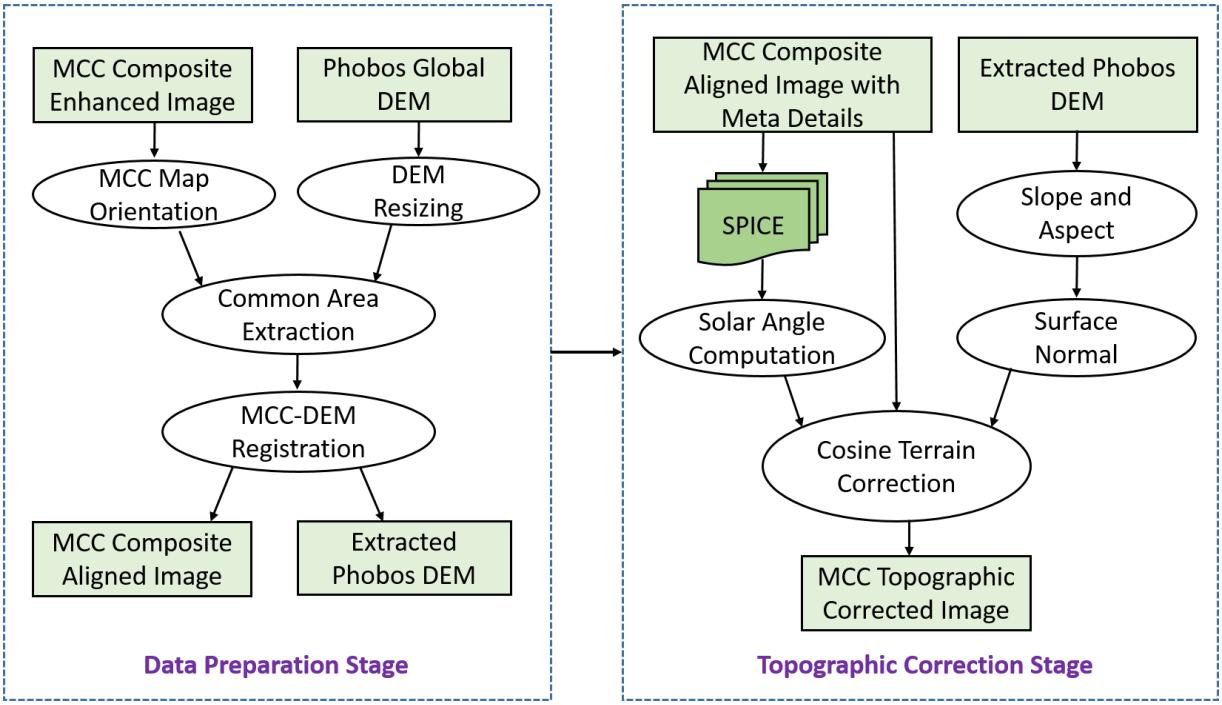

Figure-7: Topographic correction framework for MCC Phobos image.

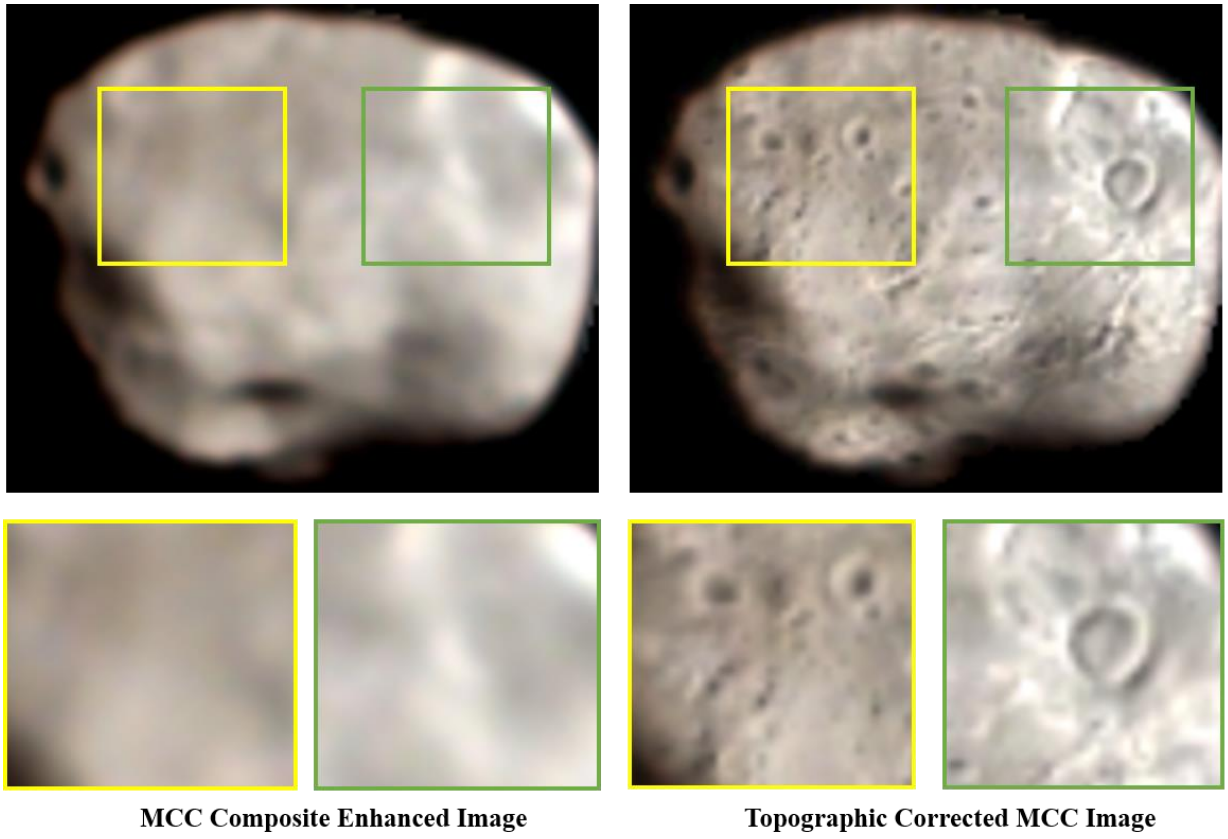

Figure-8: Topographic correction applied to MCC Phobos image.

7. Enhanced Phobos Image Assessment and Feature Identification

The MCC images can be compared with USGS Phobos global image as generated using high resolution image of Viking orbiter [55]. Here, this Phobos image map can be considered as a reference image while computing quantitative metrics, such as Root Mean Square Error (RMSE), Peak Signal to Noise Ratio (PSNR) and Structural Similarity Index Map (SSIM) [56]. The region of interest in reference image is cropped and resampled to MCC spatial resolution for better analysis. Table-3 shows the image quality metrics computed for the enhanced image and topographically corrected image. In accordance with qualitative evaluation, the RMSE is relatively less after topographic correction. The other parameters, such as PSNR and SSIM are high in the super resolved image as compared to enhanced image. To compare the quality of the final image, no reference based image spatial quality assessment, namely BRISQUE is computed before and after topographic correction. The model score is shown in Table-4, which indicates that topographically corrected image has low score. In BRISQUE model, low score indicates better image quality than the enhanced image.

Table-4 Comparison of MCC image quality metrics.

S.No	MCC Image Detail	RMSE	PSNR	SSIM	BRISQUE Model Score
1.	MCC Enhanced Image	92.66	8.79	0.18	53.75
2.	MCC Topographically Corrected Image	89.56	9.08	0.49	19.85

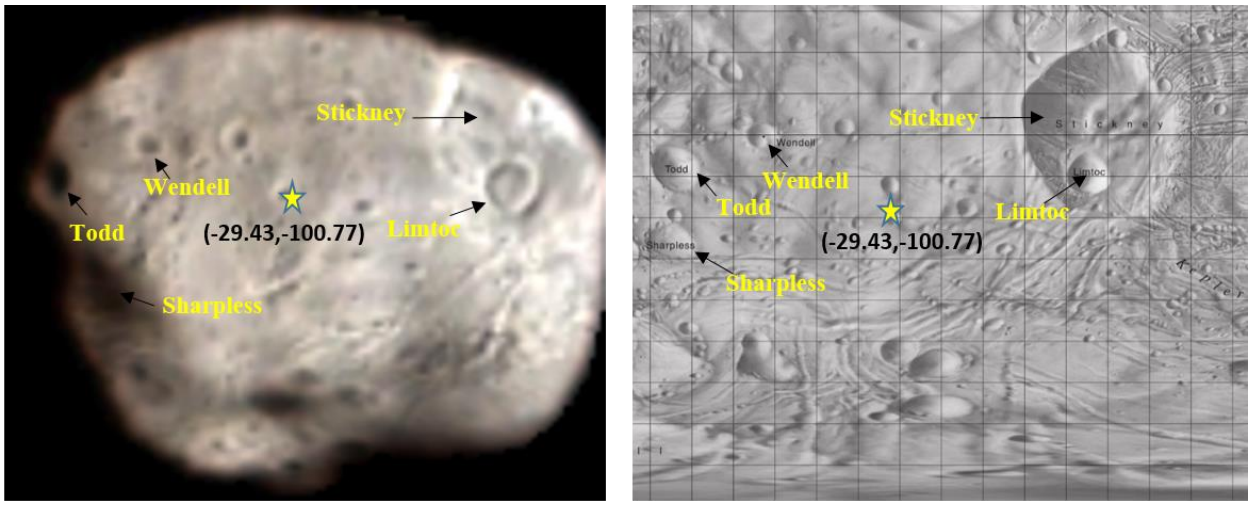

Super Resolved MCC Phobos Image **Phobos Nomenclature Image (Source: USGS)**

Figure-9: MCC Phobos Annotated Image validation with Phobos Nomenclature map

The computed coordinates using SPICE toolkit helps in determining the central location of the image. It lies between Stickney and Todd features of Phobos. Sharpless is also discernible below Todd. Adjacent to Todd, Windell is visible in the super resolved image. Figure-9 shows the MCC Phobos super resolved annotated image and its validation with USGS nomenclature map [19].

8. Conclusion

Recent MCC Phobos imaging is an interesting opportunity for planetary scientists to study the surface features of Phobos including craters and groove like structures [9]. This paper describes the image processing technique to process multiple MCC frames in order to generate a super resolved image. The software package for image enhancement was implemented in C++ and Linux operating system environment. The developed processing workflow was rigorously tested using unpaired MCC images. Further, the execution time was found to be approximately a minute while generating the MCC enhanced image in automatic mode. R-SIFT based feature matching was found to be an efficient way to align MCC frames at an accuracy equivalent sub-pixel level registration. Medoid composite representation and CLAHE based enhancement boosted the

contrast of local targets. Topographic correction procedure assisted in normalizing the radiometry of MCC composite image. Topographically corrected Phobos image was found to have highly resolved surface features across different slopes. The image quality parameters quantified the improvement in the final image. The super resolved Phobos image was compared with available MRO and Mars Express images for visual assessment, and it was found to be at par in terms of spatial characteristics at the same resolution. The enhanced image was validated with the labeled map of Phobos at desired locations. It is worth emphasizing that the established pipeline is likely to pave the way for enhancement of unpaired planetary images, suggesting benefits in scientific studies upon further analysis. In future, it is intended to generate a digital image model of Mars using the publicly available archive of MCC [57].

Acknowledgement

The authors would like to thank the Director, Space Applications Centre (SAC), ISRO for his encouragement to work on planetary data. The authors thank ISSDC team, Byalalu, India for providing MCC Phobos image datasets to conduct this activity. The authors acknowledge the efforts of MOM team, payload team, data processing team, and science team for acquiring the image of Phobos using MCC. The authors thank MOM operation team for smooth access of MCC images and SPICE Kernels through National Knowledge Network (NKN) and MOM Long Term Archive web browse portal https://mrbrowse.issdc.gov.in/MOMLTA. The authors also thank other team members of Optical Data Processing Division, Space Applications Centre (ISRO) for providing valuable feedback throughout this research.

References

1. Masursky, H. (1973). An overview of geological results from Mariner 9. Journal of Geophysical Research, 78(20), 4009-4030.

2. Zurek, R. W., & Smrekar, S. E. (2007). An overview of the Mars Reconnaissance Orbiter (MRO) science mission. Journal of Geophysical Research: Planets, 112(E5).

3. Jaumann, R., Neukum, G., Behnke, T., Duxbury, T. C., Eichentopf, K., Flohrer, J., ... & HRSC Co-Investigator Team. (2007). The high-resolution stereo camera (HRSC) experiment on Mars Express: Instrument aspects and experiment conduct from interplanetary cruise through the nominal mission. Planetary and Space Science, 55(7-8), 928-952.

4. Chicarro, A., Martin, P., & Trautner, R. (2004, August). The Mars Express mission: an overview. In Mars Express: The Scientific Payload (Vol. 1240, pp. 3-13).

5. Witasse, O., Duxbury, T., Chicarro, A., Altobelli, N., Andert, T., Aronica, A., ... & Zegers, T. (2014). Mars express investigations of Phobos and Deimos. Planetary and Space Science, 102, 18-34.

6. Rosenblatt, P., Charnoz, S., Dunseath, K. M., Terao-Dunseath, M., Trinh, A., Hyodo, R., ... & Toupin, S. (2016). Accretion of Phobos and Deimos in an extended debris disc stirred by transient moons. Nature Geoscience, 9(8), 581-583.

7. Le Maistre, S., Rosenblatt, P., Rambaux, N., Castillo-Rogez, J. C., Dehant, V., & Marty, J. C. (2013). Phobos interior from librations determination using Doppler and star tracker measurements. Planetary and Space Science, 85, 106-122.

8. Hyodo, R., Genda, H., Charnoz, S., & Rosenblatt, P. (2017). On the impact origin of Phobos and Deimos. I. Thermodynamic and physical aspects. The Astrophysical Journal, 845(2), 125.

9. Duxbury, T. C., Zakharov, A. V., Hoffmann, H., & Guinness, E. A. (2014). Spacecraft exploration of Phobos and Deimos. *Planetary and Space Science*, 102, 9-17.

10. Arunan, S., & Satish, R. (2015). Mars Orbiter Mission spacecraft and its challenges. *Current Science*, 1061-1069.

11. Arya, A. S., Sarkar, S. S., Srinivas, A. R., Moorthi, S. M., Patel, V. D., Singh, R. B., ... & Shah, D. (2015). Mars Colour Camera: the payload characterization/calibration and data analysis from Earth imaging phase. *Current Science*, 109.

12. Menon, D., & Calvagno, G. (2011). Color image demosaicking: An overview. *Signal Processing: Image Communication*, 26(8-9), 518-533.

13. Kwan, C., & Chou, B. (2019). A comparative study of conventional and deep learning approaches for demosaicing Mastcam images. In Signal Processing, Sensor/Information Fusion, and Target Recognition XXVIII (Vol. 11018, p. 1101814). *International Society for Optics and Photonics*.

14. McMahon, S. K. (1996). Overview of the planetary data system. *Planetary and Space Science*, 44(1), 3-12.

15. Brown, L. G. (1992). A survey of image registration techniques. *ACM computing surveys (CSUR)*, 24(4), 325-376.

16. Wang, D. C., Vagnucci, A. H., & Li, C. C. (1983). Digital image enhancement: a survey. *Computer vision, graphics, and image processing*, 24(3), 363-381.

17. Acton Jr, C. H. (1996). Ancillary data services of NASA's navigation and ancillary information facility. *Planetary and Space Science*, 44(1), 65-70.

18. Richter, R., Kellenberger, T., & Kaufmann, H. (2009). Comparison of topographic correction methods. *Remote Sensing*, 1(3), 184-196.

19. https://astrogeology.usgs.gov/search/map/Phobos/Nomenclature/phobos-cylindrical-grid (Accessed on 18 September 2020)

20. Gaddis, L., Anderson, J., Becker, K., Becker, T., Cook, D., Edwards, K., ... & Robinson, M. (1997, March). An overview of the integrated software for imaging spectrometers (ISIS). In Lunar and Planetary Science Conference (Vol. 28, p. 387).

21. Moratto, Z. M., Broxton, M. J., Beyer, R. A., Lundy, M., & Husmann, K. (2010). Ames Stereo Pipeline, NASA's open source automated stereogrammetry software. LPI, (1533), 2364.

22. Troglio, G., Le Moigne, J., Benediktsson, J. A., Moser, G., & Serpico, S. B. (2011). Automatic extraction of ellipsoidal features for planetary image registration. *IEEE Geoscience and remote sensing letters*, 9(1), 95-99.

23. Harris, C. G., & Stephens, M. (1988, August). A combined corner and edge detector. In *Alvey vision conference* (Vol. 15, No. 50, pp. 10-5244).

24. Rublee, E., Rabaud, V., Konolige, K., & Bradski, G. (2011, November). ORB: An efficient alternative to SIFT or SURF. In *2011 International conference on computer vision* (pp. 2564-2571). Ieee.

25. Bay, H., Tuytelaars, T., & Van Gool, L. (2006, May). Surf: Speeded up robust features. In *European conference on computer vision* (pp. 404-417). Springer, Berlin, Heidelberg.

26. Lowe, D. G. (2004). Distinctive image features from scale-invariant keypoints. *International journal of computer vision*, 60(2), 91-110.

27. Misra, I., Sharma, V., Moorthi, S. M., & Dhar, D. (2019). An approach for generation of multi temporal co-registered optical remote sensing images from Resourcesat-2/2A sensors. Journal of Geomatics, 13(1).

28. Xin, X., Liu, B., Di, K., Jia, M., & Oberst, J. (2018). High-precision co-registration of orbiter imagery and digital elevation model constrained by both geometric and photometric information. *ISPRS Journal of Photogrammetry and Remote Sensing*, 144, 28-37.

29. Ma, W., Wen, Z., Wu, Y., Jiao, L., Gong, M., Zheng, Y., & Liu, L. (2016). Remote sensing image registration with modified SIFT and enhanced feature matching. *IEEE Geoscience and Remote Sensing Letters*, *14*(1), 3-7.

30. Estivill-Castrol, V., & Murray, A. T. (1998, April). Discovering associations in spatial data—an efficient medoid based approach. *In Pacific-Asia Conference on Knowledge Discovery and Data Mining* (pp. 110-121). Springer, Berlin, Heidelberg.

31. Zhang, Q., & Couloigner, I. (2005, May). A new and efficient k-medoid algorithm for spatial clustering. *In International conference on computational science and its applications* (pp. 181-189). Springer, Berlin, Heidelberg.

32. Azzari, G., & Lobell, D. B. (2017). Landsat-based classification in the cloud: An opportunity for a paradigm shift in land cover monitoring. *Remote Sensing of Environment*, 202, 64-74.

33. Blount, G., & Greeley, R. (1987, June). Correlated noise as a planetary image enhancement technique. *In Bulletin of the American Astronomical Society* (Vol. 19, p. 847).

34. Prashar, A., Moorthi, S. M., Roy,S. & Arya,A.S. (2015, September). Mars Color Camera Experimenter to Archive Interface Control Document [EAICD] ISRO Science Data Archive. Document No: MCC-SAC-EAICD-01.

35. Bolles, R. C., & Fischler, M. A. (1981). A RANSAC-based approach to model fitting and its application to finding cylinders in range data. *In IJCAI* (Vol. 1981, pp. 637-643).

36. Li, Q., Wang, G., Liu, J., & Chen, S. (2009). Robust scale-invariant feature matching for remote sensing image registration. *IEEE Geoscience and Remote Sensing Letters*, 6(2), 287-291

37. Ma, W., Wen, Z., Wu, Y., Jiao, L., Gong, M., Zheng, Y., & Liu, L. (2016). Remote sensing image registration with modified SIFT and enhanced feature matching. *IEEE Geoscience and Remote Sensing Letters*, 14(1), 3-7.

38. Wu, B., Zeng, H., & Hu, H. (2018). Illumination invariant feature point matching for high-resolution planetary remote sensing images. *Planetary and Space Science*, 152, 45-54.

39. Derpanis, K. G. (2010). Overview of the RANSAC Algorithm. *Image Rochester NY*, 4(1), 2-3.

40. Chai, T., & Draxler, R. R. (2014). Root mean square error (RMSE) or mean absolute error (MAE)?. *GMDD*, 7(1), 1525-1534.

41. Flood, N. (2013). Seasonal composite Landsat TM/ETM+ images using the medoid (a multi-dimensional median). *Remote Sensing*, 5(12), 6481-6500.

42. Tuomisto, H. (2016). Influence of compositing criterion and data availability on pixel-based Landsat TM/ETM+ image compositing over Amazonian forests. *IEEE Journal of Selected Topics in Applied Earth Observations and Remote Sensing*, 10(3), 857-867.

43. Van doninck, J., & Tuomisto, H. (2018). A Landsat composite covering all Amazonia for applications in ecology and conservation. *Remote Sensing in Ecology and Conservation*, 4(3), 197-210.

44. Reza, A. M. (2004). Realization of the contrast limited adaptive histogram equalization (CLAHE) for real-time image enhancement. *Journal of VLSI signal processing systems for signal, image and video technology*, 38(1), 35-44.

45. Setiawan, A. W., Mengko, T. R., Santoso, O. S., & Suksmono, A. B. (2013). Color retinal image enhancement using CLAHE. *In International Conference on ICT for Smart Society* (pp. 1-3). IEEE.

46. Li, L., Si, Y., & Jia, Z. (2018). Medical image enhancement based on CLAHE and unsharp masking in NSCT domain. *Journal of Medical Imaging and Health Informatics*, 8(3), 431-438.

47. Mittal, A., Moorthy, A. K., & Bovik, A. C. (2012). No-reference image quality assessment in the spatial domain. *IEEE Transactions on image processing*, 21(12), 4695-4708.

48. Acton, C., Bachman, N., Diaz Del Rio, J., Semenov, B., Wright, E., & Yamamoto, Y. (2011, October). Spice: A means for determining observation geometry. *In EPSC–DPS Joint Meeting*.

49. Acton Jr, C. H. (1990). The SPICE concept-An approach to providing geometric and other ancillary information needed for interpretation of data returned from space science instruments. sis.

50. Acton, C., Bachman, N., Semenov, B., & Wright, E. (2018). A look towards the future in the handling of space science mission geometry. *Planetary and Space Science*, 150, 9-12.

51. Colby, J. D. (1991). Topographic normalization in rugged terrain. *Photogrammetric Engineering and Remote Sensing*, 57(5), 531-537.

52. Richter, R., & Schläpfer, D. (2005). Atmospheric/topographic correction for satellite imagery. *DLR report DLR-IB*, 565.

53. Hantson, S., & Chuvieco, E. (2011). Evaluation of different topographic correction methods for Landsat imagery. *International Journal of Applied Earth Observation and Geoinformation*, 13(5), 691-700.

54. Willner, K., Oberst, J., Hussmann, H., Giese, B., Hoffman, H., Matz, K.-D., Roatsch, T., & Duxbury, T. (2010). Phobos control point network, rotation, and shape. *Earth and Planetary Science Letters*, 294(3–4), 541-546. https://doi.org/10.1016/j.epsl.2009.07.033

55. Wählisch, M., Willner, K., Oberst, J., Matz, K. D., Scholten, F., Roatsch, T., Hoffmann, H., Semm, S. & Neukum, G. (2010). A new topographic image atlas of Phobos. *Earth and Planetary Science Letters*, 294(3-4), 547-553.

56. Wang, Z., Bovik, A. C., Sheikh, H. R., & Simoncelli, E. P. (2004). Image quality assessment: from error visibility to structural similarity. *IEEE transactions on image processing*, 13(4), 600-612.

57. Moorthi, S. M., Arya, A. S., Mathew, K., Singh, R. P., Chauhan, P., Sarkar, S. S., ... & Kiran Kumar, A. S. (2015). Mars Orbiter Mission: Science Data Products and Archive Pipeline. In *Lunar and Planetary Science Conference*, No. 1832, p. 1317.